

Modern Physics Letters B  
 © World Scientific Publishing Company

## FREE EXPANSION OF IMPENETRABLE BOSONS ON ONE-DIMENSIONAL OPTICAL LATTICES

MARCOS RIGOL

*Physics Department, University of California, Davis, CA 95616, USA*

ALEJANDRO MURAMATSU

*Institut für Theoretische Physik III, Universität Stuttgart, 70550 Stuttgart, Germany*

Received (Day Month Year)

Revised (Day Month Year)

We review recent exact results for the free expansion of impenetrable bosons on one-dimensional lattices, after switching off a confining potential. When the system is initially in a superfluid state, far from the regime in which the Mott-insulator appears in the middle of the trap, the momentum distribution of the expanding bosons rapidly approaches the momentum distribution of noninteracting fermions. Remarkably, no loss in coherence is observed in the system as reflected by a large occupation of the lowest eigenstate of the one-particle density matrix. In the opposite limit, when the initial system is a pure Mott insulator with one particle per lattice site, the expansion leads to the emergence of quasicondensates at finite momentum. In this case, one-particle correlations like the ones shown to be universal in the equilibrium case develop in the system. We show that the out-of-equilibrium behavior of the Shannon information entropy in momentum space, and its contrast with the one of noninteracting fermions, allows to differentiate the two different regimes of interest. It also helps in understanding the crossover between them.

*Keywords:* nonequilibrium; hardcore; fermionization.

### 1. Introduction

Physical systems displaying the effects of a reduced dimensionality have been increasingly attracting the interest of experimental and theoretical physicists in the past decades. Traditionally a condensed-matter subject, it has received a lot of attention within the last years in the framework of ultracold quantum gases. The realization of Bose-Einstein condensates (BEC) in very anisotropic traps,<sup>1,2,3</sup> or their loading on optical lattices,<sup>4,5,6,7,8,9,10</sup> allow experimentalists to obtain a rich variety of (quasi-)one-dimensional (1D) systems where the reduced dimensionality rules the physics.

In particular, the 1D regime where bosons behave as impenetrable particles,<sup>8,9</sup> also known as hardcore bosons (HCB's), has generated much interest recently. This regime, which has been called the Tonks-Girardeau (TG) regime,<sup>11</sup> can be obtained for large positive three-dimensional scattering lengths, low densities, and

low temperatures.<sup>12,13,14</sup> Contrary to weakly interacting bosons, HCB's in 1D share many properties with noninteracting spinless fermions to which they can be mapped.<sup>11</sup> (The TG regime is sometimes referred as the fermionized regime.) Properties like the energy, density profiles, and density-density correlations, are identical in both systems. On the contrary, one-particle correlations, and related quantities like the momentum distribution function ( $n_k$ ), and the so-called natural orbitals, are very different.

The 1D TG gas, introduced by Girardeau in the 60's,<sup>11</sup> has been extensively studied in the literature by means of different techniques, both in homogeneous,<sup>15,16,17,18,19,20</sup> and harmonically trapped<sup>21,22,23,24</sup> systems. In 1D, even at zero temperature, HCB's do not exhibit BEC. As shown by Lenard,<sup>16</sup> and Vaidya and Tracy,<sup>17</sup> one-particle correlations decay with a power law  $\rho_x \sim 1/\sqrt{x}$ . Hence, the highest occupied effective single-particle state (the lowest natural orbital) in the system has an occupation  $\lambda_0 \sim \sqrt{N_b}$  ( $N_b$  being the number of bosons), i.e.,  $\lambda_0 \rightarrow \infty$  for  $N_b \rightarrow \infty$ , but  $\lambda_0/N_b \rightarrow 0$ , and we call this state a quasicondensate. A similar result has been obtained in harmonic traps.<sup>23</sup>

Once the 1D regime has been achieved experimentally, for example by means of a two-dimensional (2D) optical lattice,<sup>4,5,7,9</sup> the addition of a new lattice along the 1D axes of the tubes<sup>8</sup> facilitates the achievement of the TG regime with respect to the continuum case. This is because it allows experimentalists to change the effective mass of the particles, and consequently the ratio between interaction and kinetic energies.<sup>8</sup> In 1D lattices the HCB Hamiltonian can be mapped onto the 1D XY model of Lieb, Schulz, and Mattis.<sup>25</sup> For periodic systems, this model has been also studied extensively in the literature,<sup>26,27,28</sup> and more recently in traps.<sup>29</sup> As in the continuum case, in a periodic lattice the HCB one-particle density matrix decays as  $\rho_x \sim 1/\sqrt{x}$  for noninteger fillings, so that the highest occupied effective single particle state has an occupation  $\sim \sqrt{N_b}$ . Remarkably, the above properties are universal independently of the power of the confining potential in the trapped case, and of the presence of Mott-insulating domains in the system.<sup>29</sup>

One fascinating possibility opened by the experimental realization of the TG regime is the study of the nonequilibrium dynamics of such strongly correlated bosonic systems. As we review in this article, two very peculiar features occur during the expansion of a HCB gas on a 1D lattice. For low initial densities, the momentum distribution of expanding HCB's rapidly approaches that of noninteracting fermions.<sup>30</sup> This occurs without any evidence of loss of coherence in the system, but rather with a slight increment of it, as reflected by the occupation of the lowest natural orbital. On the other hand, when the system starts its free evolution from a pure Mott-insulating (Fock) state, quasicondensates of HCB's emerge at finite momentum.<sup>31</sup>

We also present in this work a detailed study of the out-of-equilibrium behavior of the Shannon information entropies<sup>32</sup> in coordinate and momentum space, for the two situations mentioned before. As the application of information concepts to the

study of correlated systems is increasing, we find that during the expansion of the TG gas in a lattice, the Shannon information entropy in momentum space displays a qualitative different behavior depending on the initial conditions in the system. This behavior allows to identify the regime where a fast fermionization of HCB momentum distribution occurs, from the one in which traveling quasicondensates are dynamically generated in the system, and study the crossover between them.

The exposition is organized as follows. In Sec. 2 we briefly describe the exact numerical approach we follow to study the nonequilibrium dynamics. We also introduce concepts that will be used in the rest of the manuscript. In Sec. 3 we analyze the dynamical fermionization of the HCB momentum distribution function. The emergence of quasicondensates at finite momentum is reviewed in Sec. 4. Section 5 is devoted to the analysis of the Shannon information entropies in coordinate and momentum space for the two cases discussed in Secs. 3 and 4, and their contrast to the ones in the fermionic case. Finally, the conclusions are presented in Sec. 6.

## 2. Exact Approach

The HCB Hamiltonian can be written as

$$H = -t \sum_i \left( b_i^\dagger b_{i+1} + h.c. \right) + V_2 \sum_i x_i^2 n_i, \quad b_i^{\dagger 2} = b_i^2 = 0, \quad \{b_i, b_i^\dagger\} = 1, \quad (1)$$

where the bosonic creation and annihilation operators at site  $i$  are denoted by  $b_i^\dagger$  and  $b_i$  respectively, and the local density operator by  $n_i = b_i^\dagger b_i$ .  $t$  is the hopping parameter, and the last term represents a harmonic trap with curvature  $V_2$  and site positions  $x_i = ia$  ( $a$  is the lattice constant). The brackets in Eq. (1) apply only to on-site anticommutation relations, for  $i \neq j$  these operators commute  $[b_i, b_j^\dagger] = 0$ .

To calculate HCB properties we use the Jordan-Wigner transformation,<sup>33</sup>

$$b_i^\dagger = f_i^\dagger \prod_{\beta=1}^{i-1} e^{-i\pi f_\beta^\dagger f_\beta}, \quad b_i = \prod_{\beta=1}^{i-1} e^{i\pi f_\beta^\dagger f_\beta} f_i, \quad (2)$$

which maps the HCB Hamiltonian onto the one of noninteracting spinless fermions

$$H_F = -t \sum_i \left( f_i^\dagger f_{i+1} + h.c. \right) + V_2 \sum_i x_i^2 n_i^f, \quad (3)$$

where  $f_i^\dagger$  and  $f_i$  are the creation and annihilation operators for spinless fermions at site  $i$ , and  $n_i^f = f_i^\dagger f_i$  is the local particle number operator.

The above mapping allows to express the equal-time Green's function for HCB's in a non-equilibrium system as

$$G_{ij}(\tau) = \langle \Psi_B(\tau) | b_i b_j^\dagger | \Psi_B(\tau) \rangle = \langle \Psi_F(\tau) | \prod_{\beta=1}^{i-1} e^{i\pi f_\beta^\dagger f_\beta} f_i f_j^\dagger \prod_{\gamma=1}^{j-1} e^{-i\pi f_\gamma^\dagger f_\gamma} | \Psi_F(\tau) \rangle, \quad (4)$$

where  $\tau$  is the real time variable,  $|\Psi_B^G(\tau)\rangle$  is the time evolving wave function for HCB's and  $|\Psi_F^G(\tau)\rangle$  is the corresponding one for noninteracting fermions.

Since there are no interactions in the equivalent fermionic system, the time evolution of an initial wave-function ( $|\Psi_F^I\rangle$ ) can be calculated numerically as

$$|\Psi_F(\tau)\rangle = e^{-iH_F\tau/\hbar}|\Psi_F^I\rangle = \prod_{\delta=1}^{N_f} \sum_{\sigma=1}^N P_{\sigma\delta}(\tau) f_{\sigma}^{\dagger} |0\rangle, \quad (5)$$

which is a product of single particle states, with  $N_f$  being the number of fermions ( $N_f = N_b$ ),  $N$  the number of lattice sites, and  $\mathbf{P}(\tau)$  the matrix of components of  $|\Psi_F(\tau)\rangle$ . Once  $|\Psi_F(\tau)\rangle$  is calculated, the action of  $\prod_{\gamma=1}^{j-1} e^{-i\pi f_{\gamma}^{\dagger} f_{\gamma}}$  on the right in Eq. (4) generates only a change of sign on the elements  $P_{\sigma\delta}(\tau)$  for  $\sigma \leq j-1$ , and the further creation of a particle at site  $j$  implies the addition of one column to  $\mathbf{P}(\tau)$  with the element  $P_{jN_f+1}(\tau) = 1$ , and all the others equal to zero. The same can be done for the action of  $\prod_{\beta=1}^{i-1} e^{i\pi f_{\beta}^{\dagger} f_{\beta}}$  on the left of Eq. (4). Hence, the HCB Green's function can be obtained as<sup>29</sup>

$$\begin{aligned} G_{ij}(\tau) &= \langle 0 | \prod_{\delta=1}^{N_f+1} \sum_{\beta=1}^N P'_{\beta\delta}{}^A(\tau) f_{\beta} \prod_{\sigma=1}^{N_f+1} \sum_{\gamma=1}^N P'_{\gamma\sigma}{}^B(\tau) f_{\gamma}^{\dagger} |0\rangle \\ &= \det \left[ \left( \mathbf{P}'^A(\tau) \right)^{\dagger} \mathbf{P}'^B(\tau) \right], \end{aligned} \quad (6)$$

where  $\mathbf{P}'^A(\tau)$  and  $\mathbf{P}'^B(\tau)$  are the new matrices calculated from  $\mathbf{P}(\tau)$  when the required signs are changed and the new columns added. The last equality in Eq. (6) is obtained after considering the following identity

$$\langle 0 | f_{\sigma_1} \cdots f_{\sigma_{N_f+1}} f_{\bar{\sigma}_{N_f+1}}^{\dagger} \cdots f_{\bar{\sigma}_1}^{\dagger} |0\rangle = \epsilon^{\lambda_1 \cdots \lambda_{N_f+1}} \delta_{\sigma_1 \bar{\sigma}_{\lambda_1}} \cdots \delta_{\sigma_{N_f+1} \bar{\sigma}_{\lambda_{N_f+1}}}, \quad (7)$$

where  $\epsilon^{\lambda_1 \cdots \lambda_{N_f+1}}$  is the Levi-Civita symbol in  $N_f + 1$  dimensions, the indices  $\lambda$  have values between one and  $N_f + 1$ .

The evaluation of  $G_{ij}(\tau)$  is done numerically, and the equal-time one-particle density matrix  $[\rho_{ij}(\tau)]$  is determined by the expression

$$\rho_{ij}(\tau) = \langle \Psi_B(\tau) | b_i^{\dagger} b_j | \Psi_B(\tau) \rangle = G_{ji}(\tau) + \delta_{ij} [1 - 2G_{ii}(\tau)]. \quad (8)$$

There are two quantities related to  $\rho_{ij}$  that will be studied here because of their relevance to experiments, and to the understanding of the coherence of the system. These quantities are the momentum distribution function ( $n_k$ ), and the so-called natural orbitals.  $n_k$  is usually obtained experimentally in time-of-flight measurements. We calculate it as

$$n_k(\tau) = (a/\zeta) \sum_{jl} e^{-ik(j-l)} \rho_{jl}(\tau), \quad \zeta = (V_2/t)^{-1/2}. \quad (9)$$

Notice that we normalize  $n_k$  using  $\zeta$ , which is a length scale set by the combination lattice-harmonic confining potential in (1). Another quantity that is relevant to define by means of  $\zeta$  is the characteristic density  $\bar{\rho} = N_b/\zeta$ .<sup>29,34</sup> It plays for trapped systems a role similar to the one of the density  $\rho = N_b/N$  in the periodic case. As  $\bar{\rho} \rightarrow 0$ , the lattice effects disappear, and one recovers the continuum limit.

On the other hand, as  $\tilde{\rho}$  increases beyond a critical value ( $\tilde{\rho}_c \sim 2.6-2.7$ ) a MI region builds up in the middle of the trap.<sup>29,34</sup>

Also of interest are the natural orbitals ( $\phi^\eta$ ). They can be considered as effective single-particle states in these strongly interacting systems, and are defined as the eigenfunctions of  $\rho_{ij}$ ,<sup>35</sup>

$$\sum_{j=1}^N \rho_{ij}(\tau) \phi_j^\eta(\tau) = \lambda_\eta(\tau) \phi_i^\eta(\tau), \quad (10)$$

having occupations  $\lambda_\eta$ . In dilute higher dimensional gases, when only the lowest natural orbital (the highest occupied one) scales  $\sim N_b$ , it can be regarded as the BEC order parameter, i.e., the condensate.<sup>36</sup> Although for periodic systems in equilibrium the natural orbitals are momentum states, this is not in general the case for trapped or out-of-equilibrium systems.

### 3. Dynamical Fermionization

In Fig. 1(a) we show the evolution of  $n_k$  for 100 HCB's once the harmonic trap confining the system is turned off. At  $\tau = 0$ , the characteristic density in the trap is  $\tilde{\rho} = 0.51$ , i.e., far from the regime with a Mott insulator. We compare the HCB  $n_k$  with the one of the equivalent noninteracting fermions  $n_k^f$  (which remains unchanged during the expansion). The Fermi momentum  $k_F$  is defined as  $\epsilon_F = -2t \cos(k_F a)$ , where  $\epsilon_F$  is the energy of the last occupied fermionic single-particle state in the trap at  $\tau = 0$ . In contrast to a periodic system, in a trap  $n_k$  is continuous at  $k_F$ . However, it approaches zero even faster than an exponential for  $k > k_F$ .

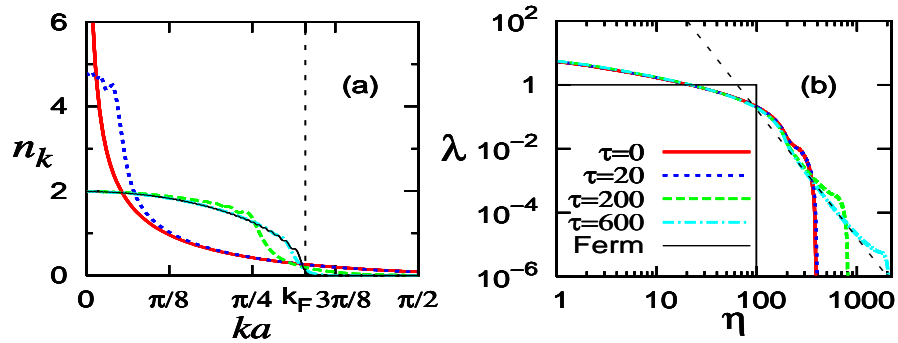


Fig. 1.  $n_k$  (a) and  $\lambda$  (b) for 100 HCB's expanding from an initial state with  $V_2 a^2 = 2.6 \times 10^{-5} t$ , and compared to the ones for the corresponding fermions. Times ( $\tau$ ) are given in units of  $\hbar/t$ . In (a),  $k_F$  denotes the Fermi momentum, and  $a$  the lattice constant. In (b), the thin dashed line corresponds to a power law  $\eta^{-4}$ , which is known from equilibrium systems (see text).

Two remarkable features are evident in Fig. 1(a). (i) Shortly after switching off the trapping potential, the peak at  $n_{k=0}$  disappears. (ii) The expansion of the system leads to an  $n_k$  for the HCB's that is equal to the one of the fermions.

This fermionization of  $n_k$  starts from the low momentum states towards  $k_F$ , and produces a Fermi edge.

After observing the above behavior of the HCB  $n_k$ , one could infer that the system is losing coherence, i.e. that the effective single-particle states obtained after diagonalizing  $\rho_{ij}$  may reduce their occupations ( $\lambda$ ) with time toward  $\lambda = 1$ , the value for noninteracting fermions. As shown in Fig. 1(b) this is not the case. The occupation of the natural orbitals almost does not change. Actually, as seen in Fig. 2(a) the lowest natural orbital occupation  $\lambda_0$  slightly increases its occupation instead of reducing it.

The out-of-equilibrium increase of  $\lambda_0$  is similar to one in the ground state when, keeping constant the number of particles, the curvature of the trap is decreased.<sup>29</sup> In both cases the increment of  $\lambda_0$  can be intuitively understood as an enhancement of the coherence in the system due to an increase of its size, which delocalize the HCB's over more lattice sites. However, in equilibrium,  $n_{k=0}$  also increases along with  $\lambda_0$ . The different behavior of  $\lambda_0$  vs  $n_{k=0}$  in- and out-of-equilibrium can be understood since in the last case the lowest natural orbital is composed by HCB's with many different momenta. This can be seen in Fig. 2(b), where we show the Fourier transform of the lowest natural orbital ( $|\phi_k^0|$ ) at different times. At  $\tau = 0$  one can see that  $|\phi_k^0|$  has a peak at  $k = 0$  showing that quasi-condensation occurs around  $k = 0$ , and this is reflected in  $n_k$ . For  $\tau > 0$  the lowest NO Fourier transform extends in  $k$ -space so that  $\phi^0$  starts to be composed by HCB's with low and large momenta, i.e., its structure changes in momentum space during the expansion.

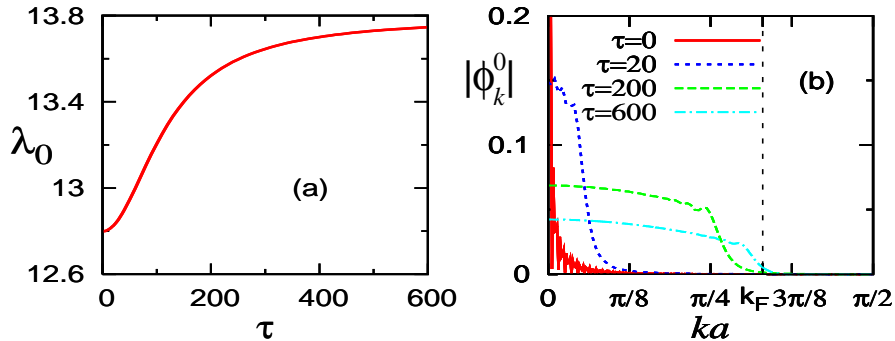


Fig. 2. Lowest natural orbital occupation (a) and the Fourier transform of the lowest natural orbital (b) for 100 HCB's expanding from an initial state with  $V_2 a^2 = 2.6 \times 10^{-5} t$ . Times ( $\tau$ ) are given in units of  $\hbar/t$ . In (b),  $k_F$  denotes de Fermi momentum.

In Fig. 1(b) there is a further salient feature, which sets in when the density of the expanding HCB's becomes very low. A decay  $\lambda_\eta \sim \eta^{-4}$  develops for large values of  $\eta$ . In equilibrium we have shown that such a power-law decay is universal at low densities, independently of the power of the confining potential.<sup>29</sup> The prefactor of the power law  $A_{N_b}$  was found to depend only on  $N_b$ .<sup>29</sup> We find out-of-equilibrium

that  $A_{N_b}$  has exactly the same value than in the ground-state.<sup>29</sup> For  $N_b = 100$  we have plotted  $\lambda_\eta = A_{N_b}\eta^{-4}$  in Fig. 1(b). Presumably, the universal decay  $\lambda_\eta \sim \eta^{-4}$  is related to the singular character of the HCB  $\delta$ -interaction, as the case for the tail  $n_k \sim |k|^{-4}$  obtained for continuous systems.<sup>37,38</sup> However, analytical proofs of this, and the universality of the prefactor  $A_{N_b}$ , have not been given so far. The power law  $n_k \sim |k|^{-4}$ , that in equilibrium<sup>29</sup> appears together with  $\lambda_\eta \sim \eta^{-4}$ , disappears during the expansion, and the HCB  $n_k$  starts to behave like the one of the fermions.

An overall understanding of the previously discussed nonequilibrium behavior of  $n_k$ , and natural orbital occupations, can be gained directly studying the one-particle density matrix. Out of equilibrium  $\rho_{ij} = |\rho_{ij}|e^{i\theta_{ij}}$ , i.e., it is complex. Results for  $\rho_{ij}$  in the same systems of Figs. 1 and 2(b) are presented in Fig. 3. Fig. 3(a) shows that  $|\rho_{ij}(\tau)|$  exhibits the same power-law decay than  $\rho_{ij}$  in the ground state,<sup>29</sup> i.e.,  $|\rho_{ij}| \sim |x_i - x_j|^{-1/2}$  for large values of  $|x_i - x_j|$  and *for all times*. Hence, this decay of the one-particle correlations is the one accounting for the large, and increasing, occupation of the lowest natural orbital as the system expands (like in the ground state). On the other hand, Figs. 3(b)-(d) show that the phase of  $\rho_{ij}$  ( $\theta_{ij}$ ) starts to increasingly oscillate at large distances. This phase is the one accounting for the fermionization of  $n_k$ . In particular, Fig. 3(b) shows that after a very short time, when the modulus of the OPDM have almost not changed,  $\theta_{ij}$  has started to oscillate for  $|x_i - x_j| \gg a$  producing a fast destruction of the zero momentum peak in  $n_k^b$ , as shown in Fig. 1(a).

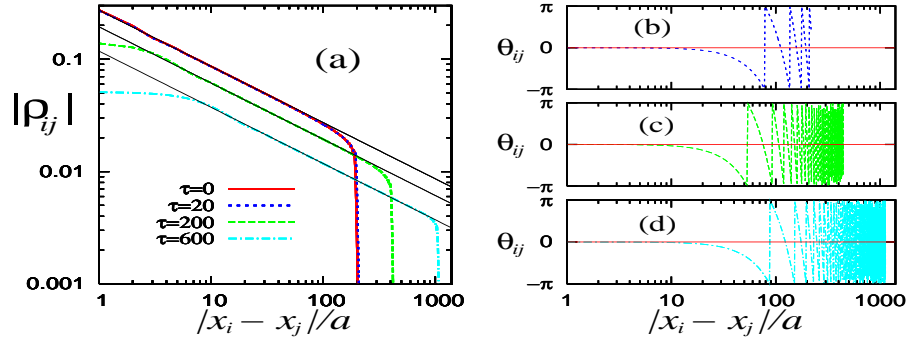


Fig. 3. Modulus of  $\rho_{ij}$  (a) and its phase (b)-(d) for the same initial trap parameters and times of Figs. 1 and 2(b). Both quantities have been calculated with respect to the center of the system. Thin continuous lines in (a) correspond to power laws  $|x_i - x_j|^{-1/2}$ .

So far we have presented results for a trap with a characteristic density  $\tilde{\rho} = 0.51$  and  $N_b = 100$ . In what follows we analyze the effects of changing  $N_b$  and  $\tilde{\rho}$  in the system. For that, we study the relative area between  $n_k$  for HCB's and  $n_k^f$  for fermions,  $\delta = (\sum_k |n_k - n_k^f|) / (\sum_k n_k)$ . We will consider that the  $n_k$  of the HCB's has fermionized when  $\delta \leq 0.05$ , i.e., when its difference with the one of the fermions is less or equal than a 5%.

In Fig. 4(a) we show  $\delta$  vs  $\tau$  in systems with  $\tilde{\rho} = 0.51$  when the number of particles in the trap is increased. Notice that keeping  $\tilde{\rho}$  constant is equivalent to keep constant the Fermi energy  $\epsilon_F$ .<sup>34</sup> Figure 4(a), and its inset, show that in this case the fermionization time ( $\tau_F$ ) increases linearly with  $N_b$ . The fast disappearance of the  $k = 0$  peak in  $n_k$  [Fig. 1(a)] is reflected in Fig. 4(a) by a fast reduction of  $\delta$ . We find that after long times the reduction of  $\delta$  is very close to a power law. This means that  $\tau_F$  depends strongly on the criterion chosen.

The consequences of increasing  $\tilde{\rho}$ , and hence the Fermi energy, are analyzed in Fig. 4(b). In order to compare systems with different  $\tilde{\rho}$ , i.e., different  $n_k$ , we display in the inset of Fig. 4(b) the ratio  $R$  between the size of the cloud when  $\delta = 0.05$ , and its initial size (before expansion). ( $R$  is independent of the number of particles for a given value of  $\tilde{\rho}$ .<sup>30</sup>) The inset in Fig. 4(b) shows that with decreasing  $\tilde{\rho}$  the ratio  $R$  reduces up to  $\sim 2.5$ . For low  $\tilde{\rho}$ , such that the interparticle distance is much larger than the lattice spacing, the initial lattice gas is equivalent to the one in continuous systems. This means that  $R \sim 2.5$  is relevant when there is no lattice, where the fermionization of  $n_k$  can be more easily observed. In continuous systems, the dynamical fermionization of the HCB  $n_k$  has been also recently studied.<sup>39,40</sup> Interestingly, the fermionization time was found to be  $\tau_F \sim 1/\epsilon_F$ ,<sup>40</sup> in contrast to our findings in the lattice where it increases linearly with  $N_b$  for a fixed  $\epsilon_F$  [inset in Fig. 4(a)], and dramatically for large characteristic densities [Fig. 4(b)].

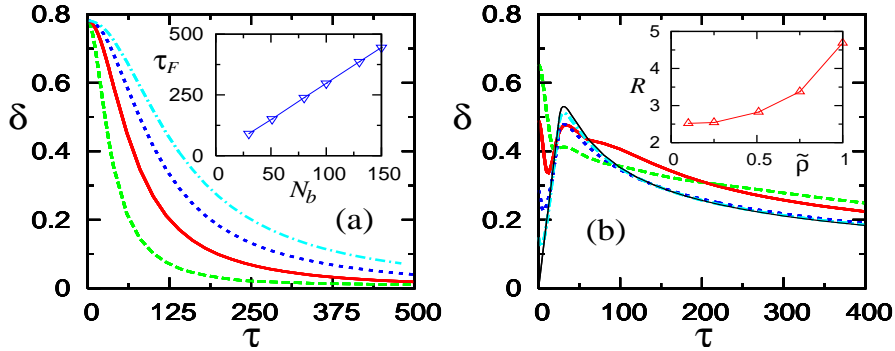


Fig. 4. Fermionization of  $n_k$  during the expansion of the gas. (a) Decrease of  $\delta$  (see text) as a function of time for  $\tilde{\rho} = 0.51$ ;  $N_b = 51$  (dashed line),  $N_b = 100$  (continuous line),  $N_b = 150$  (dotted line), and  $N_b = 200$  (dashed-dotted line). The inset shows the fermionization time  $\tau_F$  (see text) vs  $N_b$ , for  $\tilde{\rho} = 0.51$ . (b) Decrease of  $\delta$  as a function of time for  $N_b = 100$ ,  $\tilde{\rho} = 2.0$  (dashed line),  $\tilde{\rho} = 2.5$  (continuous line); and  $N_b = 101$ ,  $\tilde{\rho} = 3.0$  (dotted line),  $\tilde{\rho} = 4.0$  (dashed-dotted line). In the last two cases there is a Mott-insulating domain in the center of the trap. We have plotted as a thin continuous line  $\delta$  vs  $\tau$  for  $N_b = 101$  in a pure Mott insulating state, i.e., a state with one particle per lattice site. The inset shows the ratio  $R$  between the size of gas when  $\delta = 0.05$  and its original size vs  $\tilde{\rho}$  for  $N_b = 100$ .

As shown in Fig. 4(b), increasing the characteristic density beyond the values depicted in its inset, the behavior of  $\delta$  starts to depart from the one seen in Fig. 4(a). This is because particles become more localized in the middle of the trap,



and after  $\tilde{\rho} \sim 2.6 - 2.7$  a Mott insulator appears in the system. This localization generates an  $n_k$  that approaches the  $n_k$  of the fermions in the initial state. [In the limit where all occupied lattice sites have  $n_i = 1$ ,  $n_k(\tau = 0) = n_k^f$ .] When such systems are released from the trap  $\delta$  increases for some time. We will study in the next section the origin of this increase. We should mention, however, that after long times a fermionization of  $n_k$  starts to occur as before for smaller  $\tilde{\rho}$ . The difference is that, as shown in Fig. 4(b), the time scales for this process are very large.

#### 4. Emergence of Quasi-Condensates at Finite Momentum

We study in this section the free expansion of HCB's that are initially in a pure Mott-insulating state with one particle per lattice site. Since double occupancy is forbidden for very large on-site repulsions  $U$ , such states can be created experimentally in very deep optical lattices, and using strong confining potentials [ $U \gg V_2(N_b a/2)^2 \gg t$ ], so that vacancies in the initial state are suppressed.

In Fig. 5 we show the evolution of density (a) and momentum (b) profiles of 301 HCB's after the confining potential is turned off. At  $\tau = 0$ ,  $n_k$  is flat corresponding to a pure Fock state, where particles are localized in real space. The corresponding  $n_k^f$  of the fermions is identical, and does not change with time. Surprisingly, sharp peaks appear in the HCB  $n_k$  at  $k = \pm\pi/2a$  during the expansion. Such peaks are very similar to the ones present at  $k = 0$  in the ground state of a system with superfluid domains.<sup>29</sup>

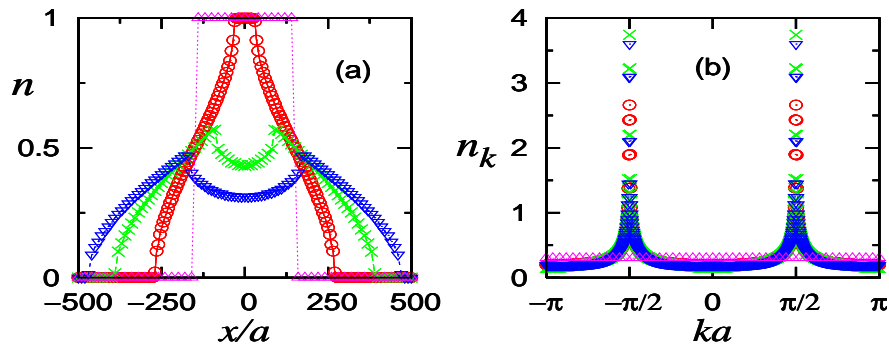


Fig. 5. Evolution of density (a) and momentum (b) profiles of 301 HCB's in 1000 lattice sites. The times are  $\tau = 0$  ( $\Delta$ ),  $60\hbar/t$  ( $\circ$ ),  $120\hbar/t$  ( $\times$ ), and  $160\hbar/t$  ( $\nabla$ ). Positions (a) and momenta (b) are normalized by the lattice constant  $a$ .

Since the peaks at  $n_{k=\pm\pi/2a}$  may indicate the presence of quasicondensates, like in the ground state, but at finite momentum in this case, we diagonalize  $\rho_{ij}$  and study the natural orbitals and their occupations. In Fig. 6(a) we show the evolution of the lowest 500 natural orbital occupations during the expansion. Like in  $n_k$ , one can see that with the disappearance of the  $\lambda = 1$  plateau, which signals the Mott insulating state, a peak appears for the highest occupied orbitals. As seen in the

inset of Fig. 6(a) (where we only show the eleven highest values of  $\lambda$ ), the two highest occupied orbitals are degenerate. We discuss below that the two peaks seen in  $n_k$  signal their emergence.

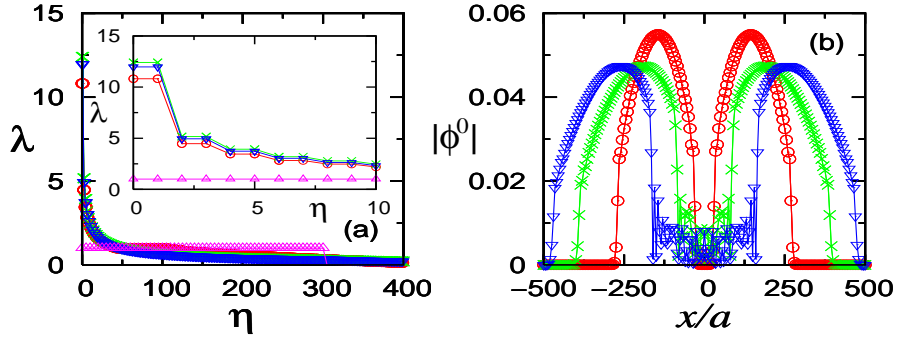


Fig. 6. Evolution of the natural orbital occupations (a) and the lowest natural orbital wave function (b) of 301 HCB's in 1000 lattice sites. The times are  $\tau = 0$  ( $\Delta$ ),  $60\hbar/t$  ( $\circ$ ),  $120\hbar/t$  ( $\times$ ), and  $160\hbar/t$  ( $\nabla$ ), and correspond to the density and momentum profiles shown in Fig. 5.

The evolution of the modulus of lowest natural orbital wave function ( $\phi^0$  is complex) is shown in Fig. 6(b). The results for  $|\phi^1|$  are identical to those of  $|\phi^0|$ . (At  $\tau = 0$  the natural orbitals are delta functions at the occupied sites, so that we do not show  $|\phi^0(\tau = 0)|$  in the figure.) As seen in Fig. 6(b) during the expansion of the HCB's, two identical wave packets (or lobes) form at the sides of the Mott insulator. Once the Mott-insulating domain has disappeared, the shape of the wave packets almost does not change, like for a soliton, and they just move in opposite directions. To show that we have superposed in Fig. 7(a) the right moving lobe at three different times. They are almost indistinguishable. This solitonic character

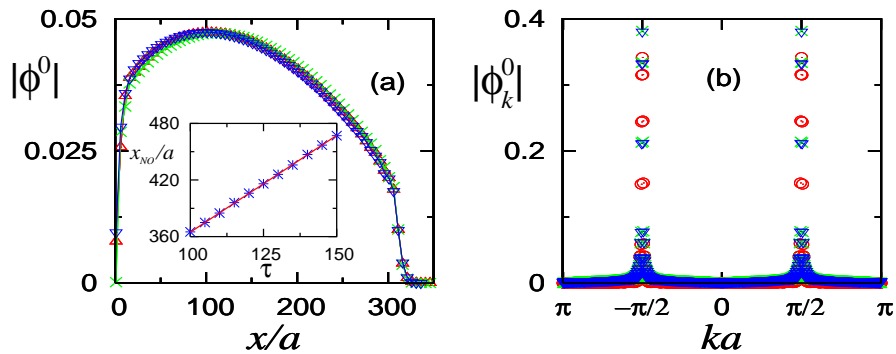


Fig. 7. (a) Superposed right lobe of the lowest natural orbital at  $\tau = 120\hbar/t$  ( $\times$ ),  $140\hbar/t$  ( $\Delta$ ), and  $160\hbar/t$  ( $\nabla$ ). The inset shows the evolution of the lowest natural orbital right lobe's position. The line going through the points has a slope 2. (b) Fourier transform of the lowest natural orbital at  $\tau = 60\hbar/t$  ( $\circ$ ),  $120\hbar/t$  ( $\times$ ), and  $160\hbar/t$  ( $\nabla$ ).

of the moving wave packets allows us to calculate their group velocity, which we find to be constant and equal to  $v_{NO} = \pm 2at/\hbar$ . This is shown in the inset of Fig. 7(a) where we have plotted the position of the right moving wave packet  $x_{NO}$  vs  $\tau$ , in units of  $\hbar/t$ , (the results for the left moving one are identical with  $x \rightarrow -x$ ), which is a straight line with slope 2. Given the HCB dispersion relation in a lattice  $\epsilon_k = -2t \cos ka$  (identical to the one of noninteracting fermions) one can obtain, using the well known expression  $v = (1/\hbar)(\partial\epsilon_k/\partial k)$ , the momenta corresponding to the moving lobes to be  $k = \pm\pi/2a$ .

The above result can be further confirmed by calculating the Fourier transform of the lowest natural orbital at different times. They are depicted in Fig. 7(b), and exhibit sharp peaks centered at quasi-momenta  $k = \pm\pi/2a$ . The peak at  $k = +\pi/2a$  appears due to the Fourier transform of the right lobe in Fig. 6(a) (i.e.  $\phi_i^0 \simeq |\phi_i^0|e^{i\pi x_i/2a}$  for  $x_i > 0$ ), and the one at  $k = -\pi/2a$  due to the Fourier transform of the left lobe (i.e.  $\phi_i^0 \simeq |\phi_i^0|e^{-i\pi x_i/2a}$  for  $x_i < 0$ ). We have also calculated the Fourier transform of the other natural orbitals finding that they have a very small or zero weight at  $k = \pm\pi/2a$ . Hence, the peaks appearing at  $n_{k=\pm\pi/2a}$  are reflecting the existence of the two traveling, with  $k = \pm\pi/2a$ , highly occupied natural orbitals.

Apart from their large occupations, the two lowest natural orbitals exhibit another remarkable property. Once formed, their moving lobes have exactly the same form independent of the number of particles ( $N_b$ ) in the initial Mott insulating state. Their size  $L$  is proportional to  $N_b$ . Actually, as shown in Fig. 8(a) the lobes can be perfectly rescaled considering  $|\varphi_0| = N_b^{1/2}|\phi^0|$  vs  $x/N_b a$ .

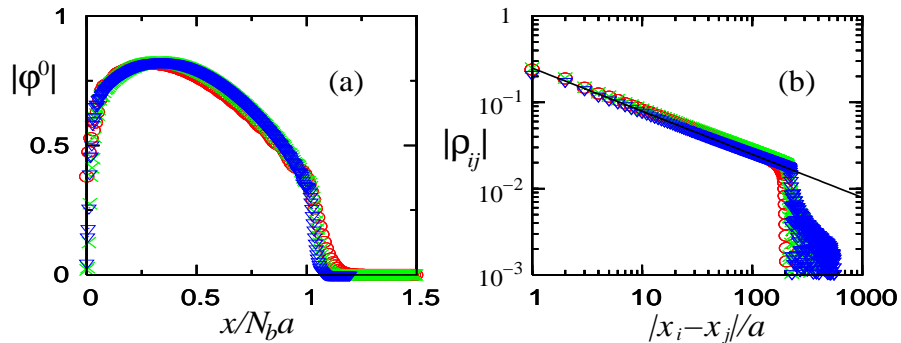


Fig. 8. (a) Scaled right lobe of the lowest natural orbital (see text) vs  $x/N_b a$  for  $N_b = 101$  ( $\circ$ ),  $201$  ( $\times$ ), and  $301$  ( $\nabla$ ). (b) One-particle density matrix measured with  $x_i$  fixed at the left extreme of the left lobe, and  $x_j > x_i$ . Times are the same of Figs. 5-7,  $\tau=60\hbar/t$  ( $\circ$ ),  $120\hbar/t$  ( $\times$ ), and  $160\hbar/t$  ( $\nabla$ ). The straight line is  $0.25 |(x_i - x_j)/a|^{-1/2}$  (see text).

In order to understand the origin of the large occupation of the two lowest natural orbitals, and their scaling properties, we study the one-particle density matrix. At  $\tau = 0$ , in the Mott insulating state,  $\rho_{ij} = \delta_{ij}$  at the occupied lattice sites, and zero in the rest of the system. During the expansion of the HCB's, a surprising

behavior sets in. Quasi-long-range one-particle correlations develop in the region of the system where the lobes of the lowest two natural orbitals were observed in Figs. 6(b)-8(a). The decay of these correlations is  $|\rho_{ij}| = 0.25 |(x_i - x_j)/a|^{-1/2}$ , as depicted in Fig. 8(b). They exhibit the same power-law decay that was shown to be universal, independent of the exponent of the trapping potential, in the ground state.<sup>29</sup> Outside the regions where the lobes are present,  $\rho_{ij}$  decays faster as seen in the tails of  $|\rho_{ij}|$  present in Fig. 8(b). These quasi-long-range correlations in two disconnected segments of the system are the reason for the degeneracy found in the lowest natural orbitals. A detailed analysis of  $\rho_{ij}$  also shows that, as expected, the peak in  $n_k$  at  $k = +\pi/2a$  is originated by components of  $\rho_{ij}$  with  $x_i, x_j > 0$ , and the one at  $k = -\pi/2a$  by the components with  $x_i, x_j < 0$ , so that in the regions of the lobes one can write  $\rho_{ij} \simeq 0.25 |(x_i - x_j)/a|^{-1/2} e^{i\pi(x_i - x_j)/2a}$  for  $x_i, x_j > 0$ , and  $\rho_{ij} \simeq 0.25 |(x_i - x_j)/a|^{-1/2} e^{-i\pi(x_i - x_j)/2a}$  for  $x_i, x_j < 0$ . The prefactor of the power law (0.25) was found to be independent of time, and of the number of particles in the initial Fock state.

Considering all the properties discussed so far one can show that the two highest occupied natural orbitals, dynamically generated and traveling with momenta  $\pm\pi/2$ , are quasicondensates in the same sense than those observed in the ground state.<sup>29</sup> They have a diverging occupation  $\lambda_0$  as the number of particles in the initial Mott insulating state increases, however  $\lambda_0/N_b \rightarrow 0$  as  $N_b \rightarrow \infty$ .  $\lambda_0$  can be obtained as

$$\begin{aligned} \lambda_0 &= \sum_{ij} \phi_i^{*0} \rho_{ij} \phi_j^0 \simeq 2/a^2 \int_0^L dx \int_0^L dy \phi^{*0}(x) \rho(x, y) \phi^0(y) \\ &= N_b^{1/2} \int_0^1 dX \int_0^1 dY \frac{|\varphi^0(X)| 0.25 |\varphi^0(Y)|}{|X - Y|^{1/2}} = A \sqrt{N_b}. \end{aligned} \quad (11)$$

The sums were replaced by integrals considering that  $L \gg a$ . In the second line of Eq. (11) we changed variables  $x = X N_b a$ ,  $y = Y N_b a$ ,  $\phi^0 = N_b^{-1/2} \varphi^0$ , and noticed that the phase factors between the natural orbital and  $\rho_{ij}$  cancel out. The integral over  $X, Y$  is a constant that we call  $A$ . The final result in Eq. (11) shows that, like in the ground state,  $\lambda_0 \sim \sqrt{N_b}$ . This result was confirmed by our numerical calculations as shown in Fig. 9(a). There we have plotted the maximum occupation of the lowest natural orbital vs  $N_b$ . A fitting of the constant  $A$  reveals a value of 0.72.

The appearance of two traveling quasicondensates, at momenta  $k = \pm\pi/2a$ , can be understood on the basis of total energy conservation. Given the HCB dispersion relation in a lattice  $\epsilon_k = -2t \cos ka$ , we notice that the total energy of the initial Mott insulating state is zero ( $E_T = 0$ ), since  $n_k$  is totally flat. Considering that the energy is conserved in the system, if all the particles would condense into one state, it would be the one with an energy corresponding to  $\bar{\epsilon}_k = E_T/N = 0$ . For the case of free expanding HCB's there are two states with  $\bar{\epsilon}_k = 0$ . They are the momentum states with  $k = \pm\pi/2a$ . Actually, in 1D there is only quasicondensation, so that the argument above applies only to maximize the occupation of the  $k = \pm\pi/2a$  states. Two other important properties of the  $k = \pm\pi/2a$  wave packets are that

they travel with the maximum velocity possible in a lattice, and that the density of states of the free system has minima at these values of  $k$ . The latter property reinforces quasicondensation into the two single  $k = \pm\pi/2a$  states.

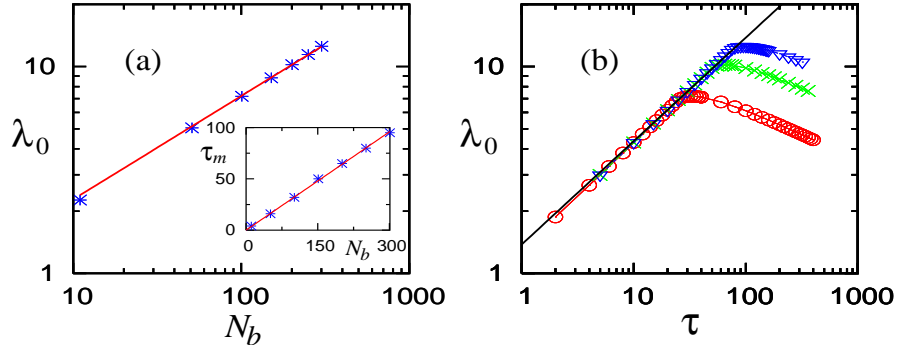


Fig. 9. (a) Maximum occupation of the lowest natural orbital vs  $N_b$ . The straight line is  $0.72 N_b^{1/2}$ . The inset shows the time at which the maximum occupation of  $\lambda_0$  is reached  $\tau_m$  (in units of  $\hbar/t$ ) vs  $N_b$ . The line following the points is  $0.32N_b$ . (b) Time evolution of the lowest NO occupation for  $N_b = 101$  ( $\circ$ ),  $201$  ( $\times$ ), and  $301$  ( $\nabla$ ). The straight line is  $1.38\sqrt{\tau t/\hbar}$ .

During the formation of the quasicondensates, the increase of their occupation is also characterized by a power law. This is shown in Fig. 9(b), where we plot  $\lambda_0$  as a function of the evolution time. The *log-log* scale evidences the fast increase of  $\lambda_0$ . A detailed examination shows that the population of the quasicondensate increases in a universal way [ $1.38\sqrt{\tau t/\hbar}$ , continuous line in Fig. 9(b)] independently of the initial number of particles in the Fock state. This power law is determined by the universal behavior of the off-diagonal part of  $\rho_{ij}$  shown before, and by the fact that during the formation of the quasicondensates, they increase their sizes linearly with time at a rate given by the maximum velocity in the lattice  $|v_{NO}| = 2at/\hbar$ . The power law mentioned before is followed up to the point where the maximal occupation is reached, which corresponds to the point at which the initial Mott insulator has completely melted. One can then realize that given  $v_{NO}$ , the time at which this occurs  $\tau_m$  depends linearly on the number of particles. We find that  $\tau_m = 0.32N_b\hbar/t$ , as shown in the inset of Fig. 9(a). To have an example of the time scales we are referring here, we consider a typical experimental setup of rubidium atoms, in a lattice with a recoil energy of  $E_r = 20\text{kHz}$ , and a depth of  $20E_r$ . In these systems, the time  $\tau_m$  can be estimated as  $\tau_m \sim 5.7N_b(\text{ms})$ .

A second characteristic of these systems that can be seen in the *log-log* plot in Fig. 9(b) is the slow reduction of the lowest natural orbital occupation, with the consequent reduction of the  $n_{k=\pm\pi/2}$  peaks. This slow reduction is consistent with the slow fermionization of  $n_k$  seen in Fig. 4(b), and suggest that such an arrangement could be used to create atom lasers with a wavelength that can be fully controlled given the lattice parameter  $a$ . No additional effort is needed to separate

the quasi-coherent part from the rest since the quasicondensate is traveling at the maximum velocity on the lattice so that the front part of the expanding cloud is the quasi-coherent part.

The actual experimental realization would imply to restrict the evolution of the initial Mott state to one direction, as shown in Fig. 10. There we display the density and momentum profiles of 150 HCB's restricted to evolve to the right in 1000 lattice sites at the same evolution times of Fig. 5. This figure shows that the values of  $n_{k=\pi/2}(\tau)$  are almost the same than the ones in Fig. 5, although the initial Fock state has half the number of particles. This is because in this case only one quasicondensate is created, so that the lowest natural orbital also has the same occupation than in Fig. 6(a), and is not degenerate anymore.

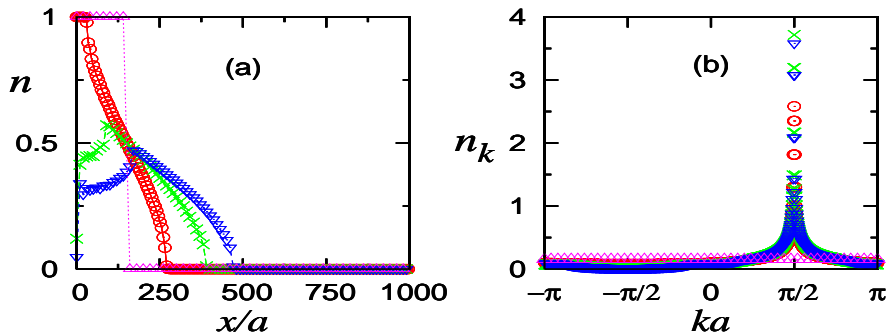


Fig. 10. Evolution of density (a) and momentum (b) profiles of 150 HCB's evolving only to the right (the system is open in the left extreme) in 1000 lattice sites. The times are  $\tau = 0$  ( $\Delta$ ),  $60\hbar/t$  ( $\circ$ ),  $120\hbar/t$  ( $\times$ ), and  $160\hbar/t$  ( $\nabla$ ).

The above results suggest how to proceed to obtain lasers in higher dimensional systems where real condensation can occur.<sup>41</sup> One could employ Mott-insulating states with one particle per lattice site created by a very strong on-site repulsive potential  $U$ . The latter is required in order to obtain a close realization of a pure Fock state, since quantum fluctuations of the particle number present in a Mott insulator for any finite  $U$  will be strongly suppressed.<sup>42,43,44</sup> Then the geometry of the lattice should be designed in order to restrict the evolution of the Mott insulator to one direction only, and to have a low density of states around the mean value of energy per particle in the initial state. With these conditions the sharp features observed in 1D may be reproduced by a condensate in higher dimensions.

## 5. Information Entropies

We study in this section the Shannon information entropies<sup>32</sup> in coordinate ( $S_n$ ) and momentum ( $S_k$ ) space for the two physical situations discussed in Secs. 3 and 4, and in between.

Here we will follow the definitions

$$S_n = - \sum_i \bar{n}_i \ln \bar{n}_i, \quad (12)$$

and

$$S_k = - \sum_k \bar{n}_k \ln \bar{n}_k, \quad (13)$$

normalizing  $\bar{n}_i$  and  $\bar{n}_k$  such that  $\sum_i \bar{n}_i = \sum_k \bar{n}_k = 1$ . Since we have studied the expansion of HCB's in systems with  $\sim 2000$  lattice sites, in all the cases discussed in this section we discretize the Brillouin zone with 2000 points to calculate  $S_k$ .

In continuous systems, the sum of  $S_n$  and  $S_k$  satisfies several interesting properties. It was rigorously proven by Bialynicki-Birula and Mycielski<sup>45</sup> that when density and momentum distributions are normalized to unity,

$$S_T = S_n + S_k \geq d(1 + \ln \pi), \quad (14)$$

with  $d$  the space dimension. At the Hartree-Fock level, it has been shown that in the ground state of atoms  $S_T$  acquires its minimum value.<sup>46</sup> And more recently, it has been proposed that  $S_T$  can be used as a measure of correlation in atomic systems.<sup>47</sup>

In what follows, the comparison of  $S_n$  and  $S_k$  with their fermionic counterparts defined in terms of the fermionic densities ( $S_n^f = - \sum_i \bar{n}_i^f \ln \bar{n}_i^f$ ) and momentum distributions ( $S_k^f = - \sum_k \bar{n}_k^f \ln \bar{n}_k^f$ ), will be shown to be very useful. Since density profiles are identical for HCB's and noninteracting fermions, at any time,  $S_n(\tau)$  and  $S_n^f(\tau)$  are the same. This identity does not hold in momentum space. In the ground state, given the large occupation of the low momentum states in the TG gas, in contrast to the extended  $n_k$  of the fermions, one can realize that  $S_k^f(\tau = 0) \geq S_k(\tau = 0)$ , where the equality only holds in the limit in which HCB's and fermions are localized in real space (the systems in Sec. 4).

We first study the behavior of  $S_n$  and  $S_k$  for the cases in which a fast fermionization of  $n_k$  was observed in Sec. 3. In Fig. 11(a) we show the evolution of  $S_n$  for systems with the same characteristic density and different  $N_b$ , like in Fig. 4(a). As the number of particles in the trap is increased keeping  $\tilde{\rho}$  constant, the initial system size increments proportionally to  $N_b$ , producing an increase of  $S_n$ . In order to compare  $S_n$  for different number of HCB's we have displaced them to coincide with  $S_n$  for  $N_b = 100$ . This can be easily achieved considering  $S_n' = S_n + \ln(100/N_b)$ . Fig. 11(a) shows that rescaling  $\tau$  by the number of particles, the time evolution of the different systems collapse over the same curve which, as expected, shows an increase of  $S_n$  as the system expands.

The behavior of  $S_k$ , for the systems in Fig. 11(a), is shown in Fig. 11(b). Since the characteristic density is kept constant, at  $\tau = 0$ ,  $S_k$  for different  $N_b$  has the same value. During the expansion one can see that  $S_k$  overcomes  $S_k^f$  (that does not change since the fermions are noninteracting). This means that, taking into account that the Shannon entropies in coordinate space are identical for HCB's

and fermions, as the TG gas expands  $S_T$  of the HCB's becomes larger than the corresponding one  $S_T^f$  of the fermions. For large times  $S_T \rightarrow S_T^f$  from above. As discussed below, the increase of  $S_T$  beyond the value of  $S_T^f$  is a characteristic of the fermionization process studied in Sec. 3.

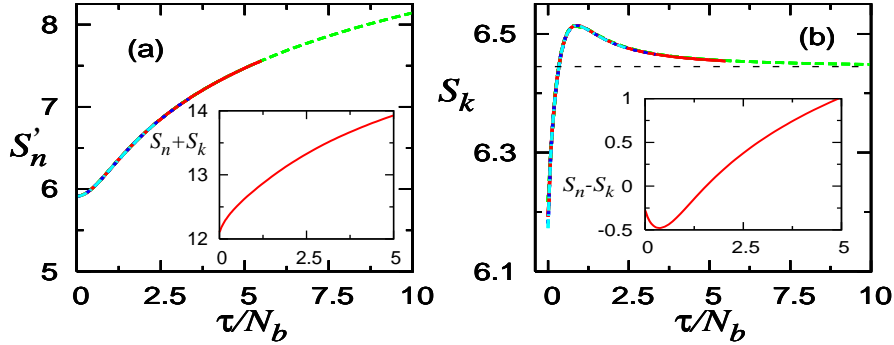


Fig. 11. Evolution of  $S'_n$  (a) and  $S_k$  (b) in systems with 2000 lattice sites. The initial state has  $\bar{\rho} = 1.0$  in all cases, and  $N_b = 51$  (dashed line),  $N_b = 100$  (continuous line),  $N_b = 150$  (dotted line), and  $N_b = 200$  (dashed-dotted line). In (a) we have displaced the  $S_n$  of  $N_b = 51$ ,  $N_b = 150$ , and  $N_b = 200$  by a constant (see text), to superpose it with the one of  $N_b = 100$ . The insets in (a) and (b) show the sum and difference, respectively, of  $S_n$  and  $S_k$  for  $N_b = 100$ . The thin dashed line in (b) shows  $S_k^f$ , which does not change in time.

We have also plotted in the insets of Figs. 11(a) and (b) the sum and differences, respectively, of  $S_n$  and  $S_k$ . The sum shows that  $S_T$  has its minimum value in the ground state. Hence, the expansion only produces its increment. The difference  $S_n - S_k$  in the inset of Figs. 11(b) reflects the fast destruction of the  $n_{k=0}$  peak at very short times, which produces changes in  $S_k$  that are larger than the ones in  $S_n$ , so that for short times  $S_k$  has the largest contribution to the increase of  $S_T$ . For large expansion times  $S_n$  is the dominant contribution to  $S_T$  as  $S_k \rightarrow S_k^f$  slowly.

The properties of the information entropies that we have discussed so far are generic for all systems that start their evolution from a state with low density in the lattice, and in which a fast fermionization of  $n_k$  occurs. Hence, we infer that they will also be valid in the continuum case,<sup>9,39,40</sup> which can be obtained as the low density limit in the lattice.<sup>29</sup> As the characteristic density in the system increases, and a Mott insulator appears in the middle of the trap, the behavior of  $S_k$  and the way in which  $S_k \rightarrow S_k^f$  change qualitatively.

In Fig. 12, we show the time evolution of  $S_n$  and  $S_k$  for a system with  $\bar{\rho} = 3.0$ , which at  $\tau = 0$  has a Mott insulating domain in the middle of the trap [Fig. 13(a)]. During the expansion of the HCB's for this initial condition  $S_n$  [Fig. 12(a)] is very similar to the one in Fig. 11(a) for low initial densities, i.e., no distinguishing feature appears in  $S_n$  for different initial densities.

On the contrary, the behavior of  $S_k$  in Fig. 13(b) is very different to the one seen in Fig. 11(b), with the exception of very short times where  $S_k$  in Fig. 13(b) exhibits



a small increase. It corresponds to the fast reduction of the  $n_{k=0}$  peak similarly to the one seen in Fig. 1(a). At  $\tau = 0$ , there is a peak at  $k = 0$  [Fig. 13(b)] because of the superfluid domains surrounding the Mott insulator in the middle of the trap [left inset in Fig. 13(a)]. At short times these superfluid regions are affected by the expansion like the systems analyzed in Sec. 3, producing an increase of  $S_k$ .

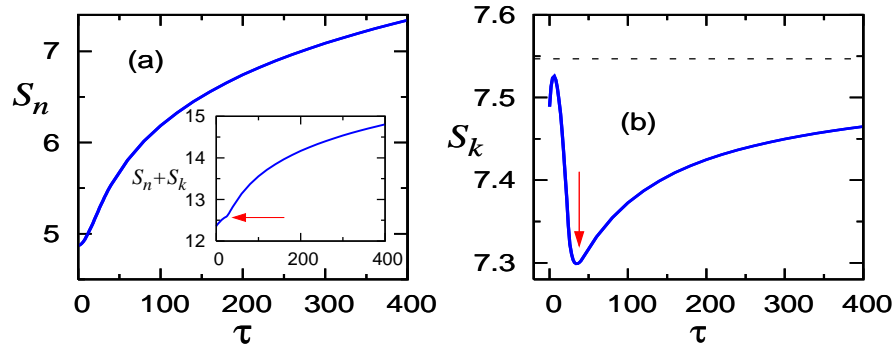


Fig. 12. Evolution of  $S_n$  (a) and  $S_k$  (b) in a system with 101 HCB's, 2000 lattice sites, and initial  $\tilde{\rho} = 3.0$ . In the inset we show the sum of  $S_n$  and  $S_k$ . The thin dashed line in (b) shows  $S_k^f$ .

With the melting of the Mott insulator in the middle of the trap, quasi-coherence builds between initially uncorrelated particles producing two peaks in  $n_k$ . As shown in Fig. 13(b) for  $\tilde{\rho} = 3$ , they are even larger than the one in the ground state. This causes the reduction of  $S_k$  seen in Fig. 12(b). Notice that the situation is similar to the one discussed in Sec. 4, but now the initial condition is different since the Mott insulator is surrounded by superfluid phases. Because of that, the peaks in  $n_k$  do not appear at  $k = \pm\pi/2$  [Fig. 13(b)], although with time they move toward  $k = \pm\pi/2$ . In this case the lowest natural orbitals are, during the expansion, more

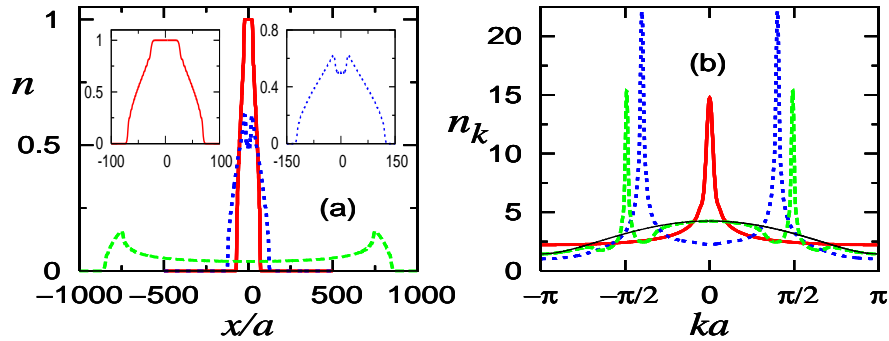


Fig. 13. Evolution of density (a) and momentum (b) profiles of 101 HCB's in 2000 lattice sites, for and initial  $\tilde{\rho} = 3.0$ . The times are  $\tau = 0$  (continuous line),  $34\hbar/t$  (dotted line),  $400\hbar/t$  (dashed line). The density profiles at  $\tau = 0$  and  $\tau = 34\hbar/t$  can be better seen in the insets in (a). In (b) we have plotted as a thin continuous line the momentum distribution function of the fermions.

complicated than the ones described in Sec. 4 since HCB's with many different momenta are couple into them. Hence, in experiments, the quality of the  $k = \pm\pi/2$  traveling quasicondensates needs to be ensured by reducing the size of the superfluid domains surrounding the Mott-insulating core.

After the peaks in  $n_k$  have acquired their maximum value,  $S_k$  starts to slowly increase towards  $n_k$ . As shown in the inset of Fig. 12(a) the sum of  $S_n$  and  $S_k$  always increases during the expansion. Even when  $S_k$  decreases, the increase of  $S_n$  is larger and warrants that the minimum of  $S_T$  occurs in the ground state. As signaled by arrows in Fig. 12, a kink can be observed in  $S_T$  when  $S_k$  attains its minimum value.

We conclude this section with the analysis of the information entropies when the system starts its evolution from pure Mott-insulating states, like the ones discussed in Sec. 4. As shown in Figs. 14(a),(b), and the inset in (a), the behavior of  $S_n$  and  $S_k$  is the same observed in Fig. 12 [if one excludes the very short times when  $S_k$  increases in Fig. 12(b) due to the superfluid domains that are not present in the case presented in Fig. 14]. Since  $S_k$  in these systems is always smaller than  $S_k^f$ , we have found a criterion in terms of the Shannon information entropy in momentum space that allows to distinguish between (i) systems in which a fast fermionization of  $n_k$  occurs (Sec. 3) where  $S_k \rightarrow S_k^f$  from above, and (ii) systems in which quasi-coherence develops dynamically producing traveling quasicondensates (Sec. 4) where  $S_k \rightarrow S_k^f$  from below. The latter feature is more difficult to see for the number of particles we have employed all over this work ( $N_b = 100-300$ ), due to the large system sizes one requires to calculate. However, in the inset in Fig. 14(b) we present results obtained for the expansion of 11 HCB's in up to 3000 lattice sites were one can clearly see that  $S_k$  is always smaller than  $S_k^f$  and that  $S_k \rightarrow S_k^f$  for very long times.

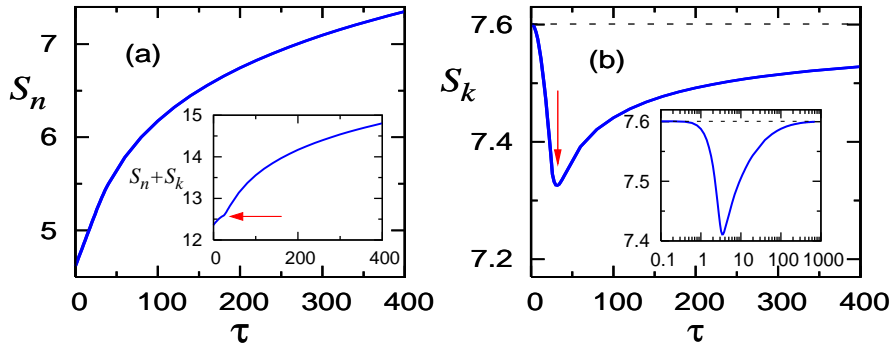


Fig. 14. Evolution of  $S_n$  (a) and  $S_k$  (b) in a system with 101 HCB's, 2000 lattice sites, and initially in a pure Mott insulating state. In the inset in (a) we show the sum of  $S_n$  and  $S_k$ . In the inset in (b) we have plotted  $S_k$  vs  $\tau$  for an initial Mott insulating state with 11 HCB's and expanding in a system with up to 3000 lattice sites. The thin dashed lines show  $S_k^f$ .

## 6. Conclusions

In this work we have presented a unified study of the expansion of TG gases in 1D optical lattices.<sup>30,31</sup> We have employed an exact numerical approach that allows to study systems with large number of particles and sizes, and for arbitrary long time scales. We find that two very different regimes can be observed according to the initial conditions of the trapped gas.

(Regime I) When the TG gas starts its free expansion from a low density system, the momentum distribution of the bosons rapidly approaches the one of the equivalent noninteracting fermions. This fermionization of  $n_k$  occurs without loss of coherence in the system. Actually, coherence increases as shown by the increase of the occupation of the lowest natural orbitals. This can be understood due to the presence of quasi-long range one-particle correlations, which have the same power-law decay as in the equilibrium case. A new feature that appears during the expansion of the gas is that the lowest natural orbital starts to be populated by particles with many different momenta, in contrast to the ground state where it is mainly populated by particles with  $k = 0$ .

(Regime II) When the TG gas starts its free expansion from a high density (Mott-insulating) trapped system, quasi-long range correlations develop between initially uncorrelated particles. They exhibit the same power-law decay known from the ground state, and produce the emergence of quasicondensates of HCB's at finite momentum. Their maximum occupation was found to be proportional to the squared root of the number of particles in the system. This quasi-condensation out-of-equilibrium is reflected by the appearance of two identical peaks in the momentum distribution function. We find that the dynamically generated quasicondensates are very similar to solitons since they can travel long distances almost without changing the shape of the wave-function and their occupation. Their momenta can be fully controlled by means of the lattice parameter.

Finally, we have shown that the Shannon information entropy in momentum space provides a criterion to distinguish the two regimes previously mentioned. In the first regime the Shannon information entropy in momentum space becomes larger than the corresponding one of the fermions, and with time approaches the last one from above. For the second regime we find that the Shannon information entropy in momentum space is always smaller for HCB's than for fermions so that the first one approaches the second one from below. (The fermionic entropy in momentum space remains unchanged during the free expansion since they are noninteracting particles.) The information entropy in momentum space was also shown to be useful to study the crossover between both regimes. It allows to distinguish the time scales in which the different processes related to the superfluid and Mott-insulating domains set in the momentum distribution function.

## 7. Acknowledgments

We are grateful to R. T. Scalettar and R. R. P. Singh for stimulating discussions. This work was supported by NSF-DMR-0312261, NSF-DMR-0240918, NSF-ITR-0313390, and SFB 382. We thank HLR-Stuttgart (Project DynMet) for allocation of computer time.

## References

1. F. Schreck, L. Khaykovich, K. L. Corwin, G. Ferrari, T. Bourdel, J. Cubizolles, and C. Salomon, *Phys. Rev. Lett.* **87** (2001) 080403.
2. A. Görlitz, J. M. Vogels, A. E. Leanhardt, C. Raman, T. L. Gustavson, J. R. Abo-Shaeer, A. P. Chikkatur, S. Gupta, S. Inouye, T. Rosenband, and W. Ketterle, *Phys. Rev. Lett.* **87** (2001) 130402.
3. T. P. Meyrath, F. Schreck, J. L. Hanssen, C.-S. Chuu, and M. G. Raizen, *Phys. Rev. A* **71** (2005) 041604(R).
4. M. Greiner, I. Bloch, O. Mandel, T. W. Hänsch, and T. Esslinger, *Phys. Rev. Lett.* **87** (2001) 160405.
5. H. Moritz, T. Stöferle, M. Köhl, and T. Esslinger, *Phys. Rev. Lett.* **91** (2003) 250402.
6. T. Stöferle, H. Moritz, C. Schori, M. Köhl, and T. Esslinger, *Phys. Rev. Lett.* **92** (2004) 130403.
7. B. L. Tolra, K. M. O'Hara, J. H. Huckans, W. D. Phillips, S. L. Rolston, and J. V. Porto, *Phys. Rev. Lett.* **92** (2004) 190401.
8. B. Paredes, A. Widera, V. Murg, O. Mandel, S. Fölling, I. Cirac, G. V. Shlyapnikov, T. W. Hänsch, and I. Bloch, *Nature* **429** (2004) 277.
9. T. Kinoshita, T. Wenger, and D. S. Weiss, *Science* **305** (2004) 1125.
10. C. D. Fertig, K. M. O'Hara, J. H. Huckans, S. L. Rolston, W. D. Phillips, and J. V. Porto, *Phys. Rev. Lett.* **94** (2005) 120403.
11. M. Girardeau, *J. Math. Phys.* **1** (1960) 516.
12. M. Olshanii, *Phys. Rev. Lett.* **81** (1998) 938.
13. D. S. Petrov, G. V. Shlyapnikov, and J. T. M. Walraven, *Phys. Rev. Lett.* **85** (2000) 3745.
14. V. Dunjko, V. Lorent, and M. Olshanii, *Phys. Rev. Lett.* **86** (2001) 5413.
15. E. H. Lieb and W. Liniger, *Phys. Rev.* **130** (1963) 1605.
16. A. Lenard, *J. Math. Phys.* **5** (1964) 930; **7** (1966) 1268.
17. H. G. Vaidya and C. A. Tracy, *Phys. Rev. Lett.* **42** (1979) 3.
18. F. D. M. Haldane, *Phys. Rev. Lett.* **47** (1981) 1840.
19. V. E. Korepin, N. M. Bogoliubov, and A. G. Izergin, *Quantum inverse scattering method and correlation functions* (Cambridge University Press, Cambridge, New York, 1993).
20. M. A. Cazalilla, *J. Phys.* **B37** (2004) S1.
21. M. D. Girardeau, E. M. Wright, and J. M. Triscari, *Phys. Rev.* **A63** (2001) 033601.
22. T. Papenbrock, *Phys. Rev.* **A67** (2003) 041601(R).
23. P. J. Forrester, N. E. Frankel, T. M. Garoni, and N. S. Witte, *Phys. Rev.* **A67** (2003) 043607.
24. D. M. Gangardt, *J. Phys.* **A37** (2004) 9335.
25. E. Lieb, T. Shultz, and D. Mattis, *Ann. Phys. (NY)* **16** (1961) 407.
26. B. M. McCoy, *Phys. Rev.* **173** (1968) 531.
27. H. G. Vaidya and C. A. Tracy, *Phys. Lett.* **A68** (1978) 378.
28. B. M. McCoy, J. H. Perk, and R. E. Schrock, *Nucl. Phys.* **B220** (1983) 35; **B220**

- (1983) 269.
29. M. Rigol and A. Muramatsu, Phys. Rev. **A70** (2004) 031603(R); **A72** (2005) 013604.
  30. M. Rigol and A. Muramatsu, Phys. Rev. Lett. **94** (2005) 240403.
  31. M. Rigol and A. Muramatsu, Phys. Rev. Lett. **93** (2004) 230404.
  32. C. E. Shannon, Bell Syst. Tech. J., **27**, 379 (1948); **27** 623 (1948).
  33. P. Jordan and E. Wigner, Z. Phys. **47** (1928) 631.
  34. M. Rigol and A. Muramatsu, Phys. Rev. **A70** (2004) 043627.
  35. O. Penrose and L. Onsager, Phys. Rev. **104** (1956) 576.
  36. A. J. Leggett, Rev. Mod. Phys. **73** (2001) 307.
  37. A. Minguzzi, P. Vignolo, and M. P. Tosi, Phys. Lett. **A294** (2002) 222.
  38. M. Olshanii and V. Dunjko, Phys. Rev. Lett. **91** (2003) 090401.
  39. B. Sutherland, Phys. Rev. Lett. **80** (1998) 3678.
  40. A. Minguzzi and D. M. Gangardt, Phys. Rev. Lett. **94** (2005) 240404.
  41. E. H. Lieb and R. Seiringer, Phys. Rev. Lett. **88** (2002) 170409.
  42. G. G. Batrouni, V. Rousseau, R. T. Scalettar, M. Rigol, A. Muramatsu, P. J. H. Denteneer, and M. Troyer, Phys. Rev. Lett. **89** (2002) 117203.
  43. M. Rigol, A. Muramatsu, G. G. Batrouni, and R. T. Scalettar, Phys. Rev. Lett. **91** (2003) 130403.
  44. M. Rigol and A. Muramatsu, Phys. Rev. **A69** (2004) 053612; Opt. Commun. **243** (2004) 33.
  45. I. Bialynicki-Birula and J. Mycielski, Commun. Math. Phys. **44** (1979) 129.
  46. S. R. Gadre, S. B. Sears, S. J. Chakravorty, and R. D. Bendale, Phys. Rev. **A32** (1985) 2602.
  47. N. L. Guevara, R. P. Sagar, and R. O. Esquivel, Phys. Rev. **A67** (2003) 012507.